Editors' Suggestion

Operational performance of crystal collimation with 6.37 *Z* TeV Pb ion beams at the LHC

M. D'Andrea,[1,*] O. Aberle,[1] R. Bruce,[1] M. Butcher,[1] M. Di Castro,[1] R. Cai,[1] I. Lamas,[1] A. Masi,[1] D. Mirarchi,[1] S. Redaelli,[1] R. Rossi,[2] and W. Scandale[2,3]

[1]*CERN, European Organization for Nuclear Research, CH-1211 Geneva 23, Switzerland*
[2]*Blackett Laboratory, Imperial College, London SW7 2AZ, United Kingdom*
[3]*INFN Sezione di Roma, Piazzale Aldo Moro 2, 00185 Rome, Italy*

(Received 4 September 2023; accepted 2 January 2024; published 25 January 2024)

The concept of crystal collimation relies on the use of bent crystals to coherently deflect positively charged particles with suitable impact conditions by trapping them in the potential well generated by adjacent crystalline planes. The resulting deflection is much higher than what can be achieved by multiple scattering on amorphous materials. For this reason, this technique has been explored in the past decades for applications to particle accelerators. In particular, a full test stand was installed in the betatron collimation insertion of the Large Hadron Collider (LHC) to explore applications to hadron beam collimation. This setup was extensively studied in Run 2 (2015–2018), as a way to improve the cleaning performance of the machine in particular with Pb ion beams, in view of the more challenging parameters envisaged for the High Luminosity upgrade (HL-LHC). This paper reports the results of measurements performed with Pb ion beams, demonstrating the capability of crystal collimation to improve the cleaning performance at the LHC. These results supported the integration of this advanced technology in the baseline upgrade program for HL-LHC.

DOI: 10.1103/PhysRevAccelBeams.27.011002

I. INTRODUCTION

The Large Hadron Collider (LHC) [1] of the European Organization for Nuclear Research (CERN) is the largest and highest-energy particle accelerator in the world. It is designed to collide counter-rotating proton or heavy-ion beams, the latter being mainly Pb ion beams [2], although a short run with Xe ions has also been performed [3], and a run with O ions is foreseen. During Run 2 (2015–2018), the maximum energy achieved was 6.5 *Z* TeV per beam for p-p and p-Pb collisions, and 6.37 *Z* TeV per beam for Pb-Pb and Xe-Xe collisions. If not properly handled, even a small fraction of the energy stored by the circulating beams (up to hundreds of MJ for protons and tens of MJ for Pb ions) can damage machine equipment or quench the superconducting magnets used to focus and bend the trajectory of the particles. A sophisticated collimation system is thus deployed to dispose of unavoidable beam losses [4–12]. The LHC layout includes two dedicated insertion regions (IRs) dedicated to intercepting particles with high betatron amplitude (IR7) and with high momentum offset (IR3). Multistage cleaning is provided via a series of collimator families, as depicted in Fig. 1: primary collimators (TCPs), secondary collimators (TCSGs), and shower absorbers (TCLAs), set at progressively larger openings around the circulating beam. Each collimator is composed of two blocks of material (carbon-fiber composite for TCPs and TCSGs and tungsten alloy for TCLAs) called *jaws*, placed at opposite sides of the beam pipe. Any primary beam losses should first hit the jaws of a TCP, and any out-scattered particles should ideally be intercepted by the TCSGs and so on, until they are all lost in safe and controlled locations [13].

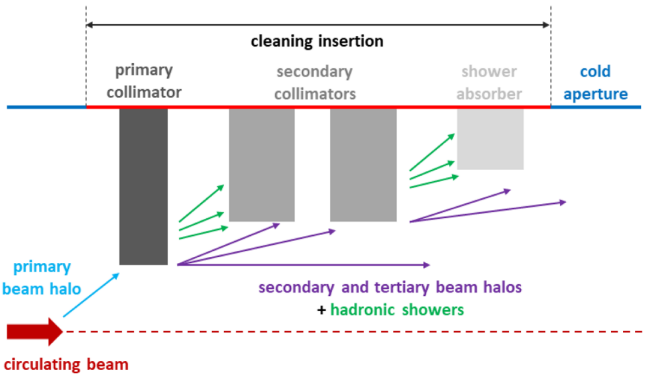

FIG. 1. Illustration of the standard collimation layout [14].

*marco.dandrea@cern.ch

TABLE I. Pb beam parameters at the start of collisions in the LHC design report, as achieved in 2018, and as envisaged for Run 3 and HL-LHC [17,28].

	LHC design	2018	Run 3	HL-LHC
Beam energy (Z TeV)	7	6.37	6.8	7
Total number of bunches	592	733	1240	1240
Bunch spacing (ns)	100	75	50	50
Bunch intensity (10^7 Pb ions)	7	21	18	18
Stored beam energy (MJ)	3.8	12.9	19.9	20.5
Normalized transverse emittance (μm)	1.5	2.3	1.65	1.65

In 2016, the High Luminosity LHC (HL-LHC) upgrade program [15,16] was approved by the CERN Council with the goal of achieving a leveled luminosity for p-p collisions of 5×10^{34} cm^{-2} s^{-1}, higher than the peak luminosity in the LHC design by a factor of 5, and resulting in a factor 10 higher integrated luminosity over the lifetime of the project. The heavy-ion physics program will also benefit from the upgrade, achieving more than a factor 6 higher luminosity [17] at the ALICE experiment [18], specializing in heavy-ion collisions. An upgrade of the collimation system is needed to cope with the new beam parameters [14]. A potential performance limitation was identified in the dispersion suppressor (DS) around IR7, where the off-momentum leakage from the upstream collimators poses risks of magnet quenches. This is particularly relevant for operation with heavy-ion beams, to which typically one month per year is dedicated, due to the factor 100 worse cleaning than for proton beams [11,19]. This degradation is caused by the large spectrum of secondary nuclei generated in fragmentation and electromagnetic dissociation processes occurring at the collimators. Because of their different charge-to-mass ratio, the resulting fragments may scatter out of the primary collimators and can escape the downstream stages, generating losses at other locations [19–21]. This is a known concern that was addressed for different machines [22,23], and the present LHC collimation system provided sufficient protection until the end of Run 2 [11,24]. However, the factor 2 higher stored energy planned for HL-LHC [17], as shown in Table I, brings the projected losses in the DS beyond the quench limit by up to a factor 5 for the assumed loss scenarios [14,25,26]. To mitigate the challenges posed by this upgrade, which for ion beams already started with Run 3 (2022–2025) [27,28], several options were investigated, such as the possibility of installing a new set of tungsten collimators in the DS to intercept off-momentum particles before they can reach the downstream magnets [29,30].

Crystal collimation was proposed as an alternative way to improve the cleaning efficiency by coherently steering beam halo particles toward a single absorber. While the deployment for operation with protons would require the design of a special absorber capable of handling the deflected halo, with heavy ions a standard secondary collimator can safely serve as a halo absorber even with HL-LHC parameters, because of the significantly lower peak power deposition [31,32]. After a successful series of preliminary studies [33,34], a review was launched in 2018 to determine the achievable performance with Pb ion beams before the end of Run 2 [35]. Thanks to the results collected in this review and described in this paper, crystal collimation was integrated into the upgrade project in December 2019 [36]. While the upgrades of the other LHC systems are sufficient to guarantee stable operation with protons in Run 3, it is currently planned to rely on crystal collimation for heavy ions.

Section II gives an overview of the principles of crystal channeling and its application to beam collimation. The main results gathered at the LHC in 2018 are reported in Secs. III and IV, which detail characterization measurements with low-intensity proton beams and cleaning performance assessment with low-intensity Pb ion beams, respectively. Section V reports the outcome of the first use of crystal collimation with high-intensity Pb ion beams. The main conclusions are then summarized in Sec. VI along with an outlook on Run 3 operation.

II. PRINCIPLES OF CRYSTAL COLLIMATION

A crystal is a material with a highly ordered atomic structure (typically, a dislocation density lower than $1/\text{cm}^2$ is required for applications to particle accelerators [37]). This *crystalline lattice* appears as a series of planes to a positively charged particle hitting the crystal with a well-aligned trajectory. The particle can then get trapped inside the electrostatic potential generated by two adjacent planes and be forced to travel in essentially empty space for the full length of the crystal [38]. The trajectory of a particle channeled by a bent crystal will be forced to follow the curvature of the crystalline planes [39], acquiring a total deflection equal to the crystal bending angle. A few millimeter long crystal can thus be used to steer charged particles by tens of μrad, an effect corresponding to an equivalent magnetic field of hundreds of Tesla over the same length at LHC energies [40]. This process, called *planar channeling*, is illustrated in Fig. 2. In the right frame, showing the potential function $U(x)$, the asymmetry between the edges of each well introduced by the curvature of the planes can be seen. This defines a *critical curvature radius*, beyond which the potential wells become so

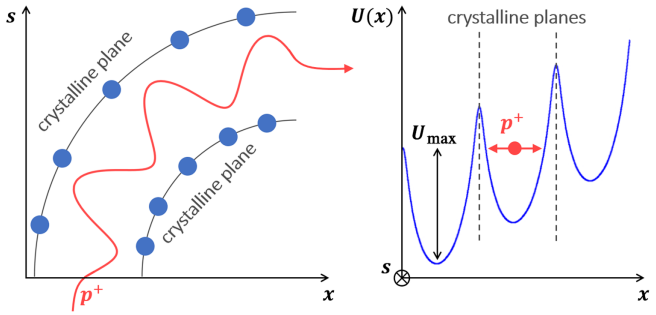

FIG. 2. Illustration of planar channeling in a bent crystal seen from the top (left) and transverse potential experienced by the proton as a function of horizontal displacement (right).

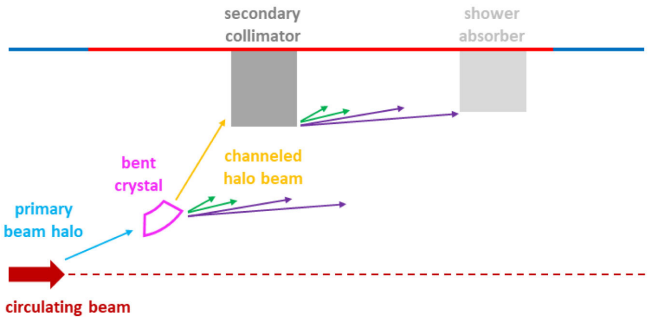

FIG. 3. Illustration of the crystal collimation layout [14].

deformed that the channeling process is not possible anymore. Furthermore, only incoming particles whose transverse energy is lower than the depth of the potential wells, and thus whose direction with respect to the crystalline planes falls within a certain angular range, have the chance to get channeled. This angular range is quantified by the *critical angle*, which depends on the energy of the impacting particle and on the crystal properties via the following formula:

$$\theta_c = \sqrt{\frac{2U_{\max}}{pv}}\left(1 - \frac{R_c}{R}\right), \tag{1}$$

where $U_{\max}$ is the depth of the potential well, p and v are the momentum and velocity of the incoming particle, respectively, R_c is the critical radius mentioned above, and R is the curvature radius of the crystal [40].

Applications of this peculiar property have been extensively studied for beam extraction [41,42] and loss shadowing [43,44] at the Super Proton Synchrotron (SPS) as well as in other machines [45], and for in-vacuum fixed target physics at the LHC [46]. Despite the first inconclusive results obtained at RHIC [47,48], crystal-assisted collimation was tested at Tevatron to successfully reduce beam losses in the detector regions [49] but was never deployed for operation. This concept was also proposed as a way to improve the cleaning performance of the LHC with protons and heavy-ion beams [50]. Pioneering validation has been carried out at CERN over the past 20 years by the UA9 collaboration [51]. In particular, results for proton beams at the LHC are reported in [52].

In a crystal-assisted collimation system, the primary collimator of each cleaning plane is replaced by a bent crystal (TCPC) placed at the edge of the circulating beam and oriented so that the crystalline planes at the crystal entry face are aligned to the beam envelope, i.e., to the direction of the individual halo particles at that amplitude (as schematically depicted in Fig. 3). Halo particles are then channeled by the crystal and deflected directly onto an absorber. This offers a number of benefits compared to a standard multistage system of amorphous collimators: (i) The probability of inelastic interactions in a crystal collimator is much lower since channeled particles travel through the empty space between planes and for a much shorter length (a few millimeters compared to tens of centimeters for a standard collimator). As a result, losses in the DS region, caused by single diffractive events in the case of proton beams and by fragmentation or electromagnetic dissociation in the case of ion beams, can be significantly reduced. Such losses constitute the main limitation of the present collimation system for operation during Run 3 and in view of HL-LHC. (ii) The channeled beam can, in principle, be directed toward a single absorber, allowing the number of stages of the collimation system to be reduced and concentrating the losses in a smaller area. (iii) Thanks to the reduced off-momentum leakage from IR7, and to the faster cleaning process, the LHC experiments can benefit from a reduction of the observed background [53]. (iv) Although this is not a limitation for ion operation at the LHC, the possibility to use less secondary collimators and open them to larger gaps translates into a reduced contribution of the collimation system to the impedance budget of the machine.

Conversely, this collimation scheme comes with the added challenge of maintaining the optimal alignment at all times. From Eq. (1), the channeling acceptance at the Run 2 LHC top energy of 6.5 TeV is of about 2.5 μrad, requiring an extremely precise angular control.

After careful design and preliminary studies at the SPS and in dedicated extraction lines [54–57], a prototype crystal collimation setup was installed in IR7 between 2015 and 2017 [58,59]. This test bench included a total of four bent Si crystals (one for each collimation plane of the two circulating beams). Each device essentially consisted of a holder that clamps the crystal, inducing a secondary curvature on the plane selected for particle steering. The mechanical bending is applied differently for the horizontal *strip crystals* and the vertical *quasimosaic crystals*, resulting in different planes used for channeling: the former ones were bent along the (110) planes while the latter ones along the (111) planes. The decision to use different kinds of crystals for this research and

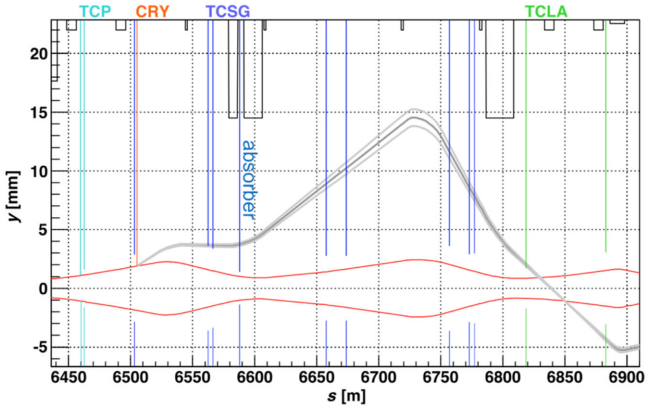

FIG. 4. Projection of the Beam 1 betatron collimation system on the vertical plane [36]. TCPs, TCSGs, TCLAs, and the vertical crystal are shown as light blue, dark blue, green, and orange bars, respectively. The beam envelope and the trajectory of the deflected halo based on the machine optics are shown in red and gray, respectively. The TCSG that intercepts the channeled halo on this plane is labeled as "absorber."

development (R&D) setup was deliberate, to assess the respective performance and define the standard to be adopted for the final devices to be used in operation. Each crystal had a length of 4 mm along the beam direction and a bending angle of 50 ± 2.5 μrad. As an example, the sequence of collimators installed in the vertical plane of Beam 1, including the crystal and the absorber of the deflected halo, can be seen in Fig. 4.

The currently installed crystal collimators are single-sided devices, with the horizontal crystals placed on the external side of the beam pipe with respect to the center of the circumference and the vertical ones installed on top. While this system can already significantly improve the cleaning performance of the machine, it cannot effectively cover specific loss scenarios involving a drift of the beam orbit. If the drift is toward the opposite side with respect to the crystal, and its size is larger than the margin between the crystal and another collimator, then the crystal cannot intercept the beam halo anymore. To address this limitation, the option to install an additional crystal collimator in each cleaning plane (on the opposite side of the current ones) was explored in a preliminary fashion, even though it would require a complete redesign of the crystal collimator assembly. However, more operational experience is needed in order to fully address this limitation and define a possible upgrade plan.

Throughout Run 2, a wide range of crystal collimation tests was performed with proton beams, ranging from establishing optimal channeling orientation and maintaining channeling through the dynamical phases of the LHC machine cycle, to the measurement of cleaning inefficiency and comparison with the standard collimation system [34,52]. The results gathered in these tests demonstrated for the first time the feasibility of the concept with multi-TeV particle beams and paved the way for tests with heavy ions (Pb and Xe) [33,34,60].

III. CRYSTAL CHARACTERIZATION WITH PROTON BEAMS

At present, the use of bent crystals for halo collimation in LHC operations with high-intensity proton beams is severely hampered by the need to design a special absorber, capable of withstanding an impacting beam loss power of the order of 1 MW over a few mm^2 caused by the high-intensity channeled beam in certain scenarios [31]. Nevertheless, activities with low-intensity proton beams are extremely important to gain experience with the setup of the system and to fully characterize the devices in a safe and controlled environment. This is particularly useful since only a very limited time is normally allocated for machine development (MD) tests with heavy-ion beams, while tests with proton beams can profit from several dedicated weeks each year. Given the low intensity allowed in these tests (up to 3×10^{11} circulating protons per beam), the jaw of a standard secondary collimator can be safely used to intercept the channeled beam halo under all circumstances.

Data for these measurements were collected using the beam loss monitoring (BLM) system, a series of more than 3900 ionization chambers installed at likely or critical loss locations of the LHC ring to detect products of showers generated by nuclear interactions of beam particles with machine elements [61]. The distribution of beam losses shows specific features when particles interact coherently with a crystal, allowing the crystal properties and performance to be evaluated.

Each crystal collimator was first inserted close to the circulating beam, using a beam-based alignment procedure similar to that used for standard collimators [9,62]. The TCP in the same plane as the crystal defines the envelope of the circulating beam by applying a cut corresponding to the desired opening (usually the nominal values of 5.7 and 5.0 in units of beam rms σ at injection and top energy, respectively). This setup is then used as a reference for the alignment of the crystal, which is inserted until the primary beam is touched (as signaled by a spike in the BLM signal at the crystal location), indicating that it is now at the same opening as the TCP. The IR7 collimators upstream of the crystal and all TCSGs located between the crystal and the secondary collimator used as absorber (see Fig. 4) are then retracted from their nominal settings by a few units of beam rms σ to have a clearer signal on the BLMs of interest.

Two types of characterization measurements were then carried out, following the well-established procedures defined in previous tests at the SPS and at the LHC [33,34,51,52,57]. During an *angular scan* (left frame of Fig. 5), each crystal was rotated at constant speed along the deflection plane. Continuous losses, intercepted by the crystal, are created during the scan using the transverse

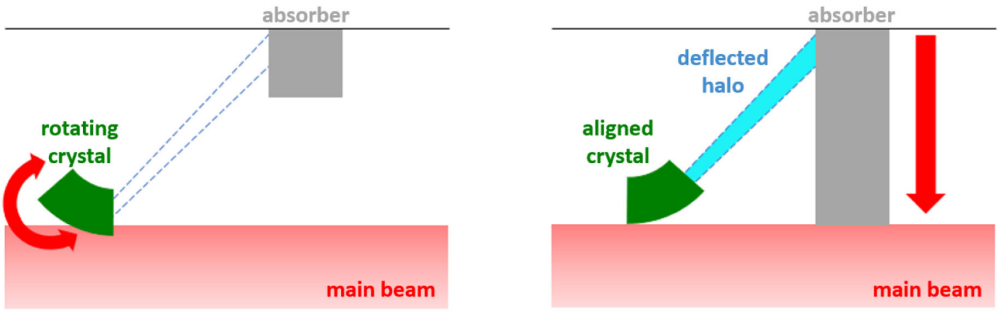

FIG. 5. Schematic representation of the angular scan (left frame) and linear scan (right frame) procedures.

damper (ADT) [63] to excite the beam with white noise and enhance the BLM response at relevant locations. An example is shown in Fig. 6. Since channeled particles have a lower probability of experiencing nuclear inelastic interactions, the BLM signal at the crystal location is reduced compared to its amorphous orientation, when no coherent processes take place and the crystal behaves like an amorphous scatterer. Conversely, the signal at the location of the absorber increases as more and more particles are deflected onto it. These features allow the orientation for which the angular alignment with the beam envelope is achieved to be identified, maximizing the probability of halo particles to be channeled. The profile of the angular scan can be compared to simulation results obtained with the multiturn tracking code SixTrack [64–67]. To reduce the effect of a nonconstant loss rate throughout the scan, the BLM signal recorded at the crystal location is normalized by the instantaneous rate of lost particles. The simulated profiles are calculated as the ratio between particles experiencing inelastic interactions in the crystal and the total number of simulated particles entering the collimation system. To allow a direct comparison, all

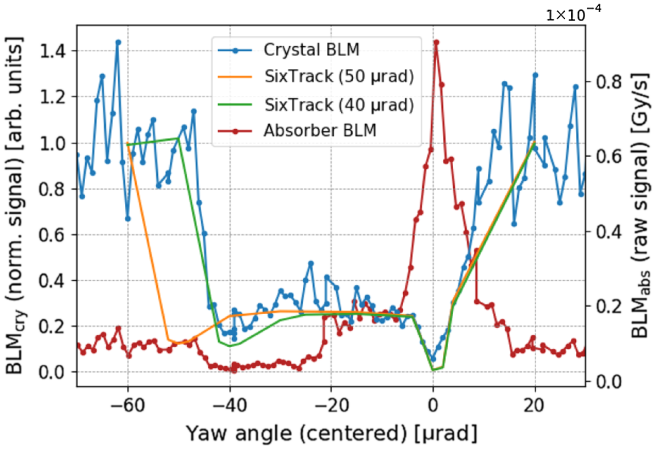

FIG. 6. Normalized BLM signal measured at the crystal location during an angular scan (horizontal crystal, Beam 2) with proton beams at 6.5 TeV, compared with SixTrack simulations for different bending angles. The raw BLM signal measured at the absorber location is also shown.

profiles are further normalized by the average signal recorded while the crystal is in the amorphous orientation (i.e., at the far sides of the scan). Since the width of the characteristic profile is proportional to the bending angle of the crystal [68], comparing the shape of the angular scan to simulations gives an estimate of this parameter.

Once the optimal channeling orientation was found, a *linear scan* of the absorber (right frame of Fig. 5) was performed by retracting the jaw used to intercept the channeled halo and progressively inserting it back toward the beam [34,57]. During this procedure, the channeled halo is intercepted by the downstream collimators, which are kept at their nominal settings. As the jaw moves toward the primary beam, the channeled halo is intercepted first, generating an increase in beam losses recorded at the collimator location. The scan is stopped as soon as the jaw touches the envelope of the primary beam, generating a massive loss spike. The recorded BLM signal is proportional to the integral of the channeled beam crossed by the jaw. By fitting the rise in signal with an error function, it is possible to extract a measure of the width of the channeled beam and of its transverse position at the absorber location. At top energy in the configuration used for these measurements, the width of the deflected beam is of the order of a few hundred μm, while its displacement with respect to the main beam is of the order of a few mm. Together with the position of the primary beam envelope, this information can then be used to reconstruct the effective deflection, i.e., the bending angle θ of the crystal, using a transfer matrix that describes the beam dynamics between the crystal and absorber locations via the optics functions of the accelerator lattice. The resulting formula is

$$\theta = \frac{\Delta x - n\sqrt{\varepsilon\beta_2}(\cos\varphi_{21} - 1)}{\sqrt{\beta_1\beta_2}\sin\varphi_{21}}, \tag{2}$$

where Δx is the measured displacement between the deflected halo and the primary beam envelope, n is the distance of the crystal from the beam center (in units of beam rms σ), ε is the beam emittance (the nominal normalized value of 3.5 μm is assumed), β is the betatronic optics function at the crystal (1) and absorber (2) location, and φ_{21} is the phase advance between the two locations.

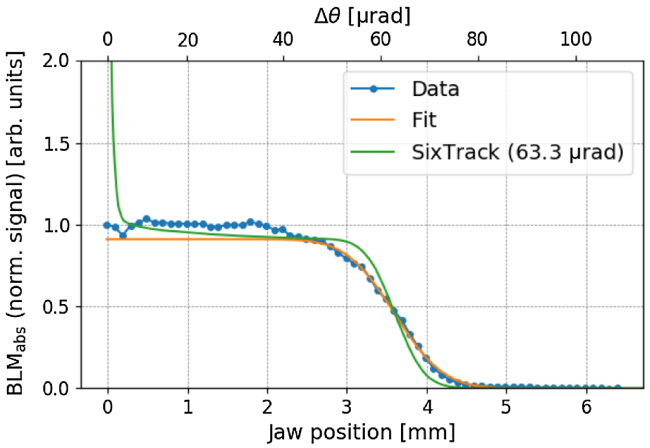

FIG. 7. Normalized BLM signal measured at the absorber location during a linear scan (horizontal crystal, Beam 1) with proton beams at 450 GeV, compared with SixTrack simulation results. The error function fit on data is also shown. The origin of the horizontal axis is set to the measured/simulated position of the beam envelope defined by the crystal.

Additionally, comparing the plateau of the error function resulting from the fit to the saturation of the BLM signal close to the primary beam envelope gives an estimate of the efficiency of the multiturn channeling process, i.e., the fraction of halo particles hitting the crystal that are actually channeled. An example is shown in Fig. 7. The measured profile is normalized by the instantaneous loss rate and by the plateau just before the primary beam is touched. The simulated profile is obtained as an integral of the particle distribution at the absorber location and is then normalized by the total number of simulated particles entering the collimation system.

These measurements are crucial to establish reference angular settings, to have early feedback on the installed crystal collimators and to identify any potential issues before tests with heavy-ion beams. The bending angle and multiturn channeling efficiency measured for each crystal at top energy in 2018 are reported in Table II. The uncertainty on the bending angle is calculated from Eq. (2) by propagating the errors on the measured quantities and the optical functions [69]. The relatively large uncertainty on the channeling efficiency comes from the high noise observed in the BLM signal when the absorber approaches the primary beam. The low efficiency of the crystal in the horizontal plane of Beam 1 is attributed to its bending angle being much larger than specification, causing an increased probability of particles losing channeling conditions before traversing the full length of the crystal at top energy [34]. The larger bending angle was due to an instability of the crystal holder and could be verified only after installation in the LHC since the Beam 1 crystals could not be characterized at the CERN experimental areas due to time constraints. This, however, should not have affected the vertical crystal on Beam 2. The low efficiency measured in this case could be related to nonoptimal conditions during the measurement, such as the fact that the only available scan was started very close to (and potentially while already partially intercepting) the deflected halo.

IV. CLEANING PERFORMANCE WITH PB ION BEAMS

A. Methods and configurations explored

Crystal channeling was observed for the first time with Pb ion beams in 2016, with a setup that included only two crystals, one for each plane of Beam 1. However, only a handful of IR7 collimator configurations could be explored, and cleaning measurements did not show a clear improvement with respect to the standard system. Following the installation of two additional crystals on Beam 2, a fully realized crystal collimation system was deployed for the first time in 2017, during the special run with Xe ion beams. Much more promising results were gathered on this occasion, and a clear reduction of IR7-DS losses could be observed using a number of different arrangements of collimator settings that allowed the performance of the system to be improved compared to previous measurements [34,51]. The 2018 ion run was then crucial, as it was the first time the full system could be tested with Pb ion beams.

A preparatory campaign of angular and linear scans, to verify key parameters of the crystals and identify the reference optimal angular orientation, was carried out with Pb ion beams at the top energy of 6.37 Z TeV before the assessment of the cleaning performance. Table III shows the bending angle and multiturn channeling efficiency measured for each crystal in 2018. The bending angle is consistent with proton measurements, while the efficiency is generally comparable or slightly lower, as expected given

TABLE II. Measured crystal parameters with 6.5 TeV proton beams. The bending angle is to be compared with the technical specification of 50 ± 2.5 μrad for all crystals.

Cleaning plane	Bending angle (μrad)	Channeling efficiency
B1H	61.3 ± 3.2	$36 \pm 6\%$
B1V	39.4 ± 2.0	$66 \pm 13\%$
B2H	36.6 ± 1.8	$68 \pm 10\%$
B2V	53.3 ± 2.7	$46 \pm 13\%$

TABLE III. Measured crystal parameters with 6.37 Z TeV Pb ion beams. The bending angle is to be compared with the technical specification of 50 ± 2.5 μrad for all crystals.

Cleaning plane	Bending angle (μrad)	Channeling efficiency
B1H	62.8 ± 3.3	$18 \pm 4\%$
B1V	40.6 ± 2.0	$61 \pm 10\%$
B2H	36.3 ± 1.8	$60 \pm 24\%$
B2V	52.9 ± 2.6	$71 \pm 14\%$

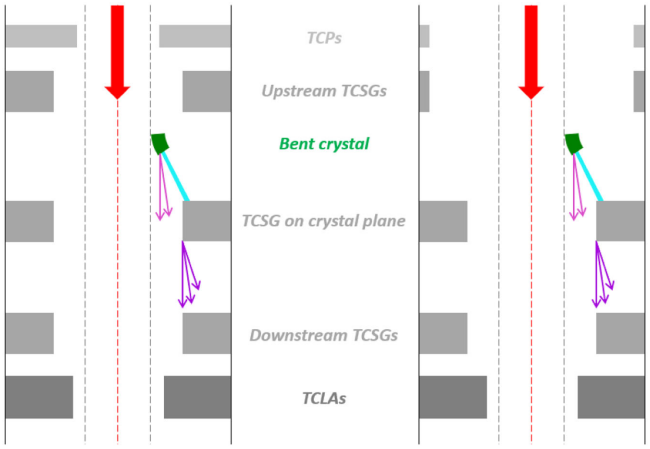

FIG. 8. Schematic representation of the collimator hierarchy used in crystal collimation tests with Pb ion beams. Primary (TCPs), secondary (TCSGs), and absorber (TCLAs) collimators are depicted in operational (left side) and MD (right side) settings. The red arrow represents the beam axis.

the different interaction dynamics. The only exception is the vertical crystal of Beam 2 which shows a higher efficiency, supporting the hypothesis of nonideal measurement conditions for this crystal with protons.

A wide range of collimator settings was explored in order to assess the achievable cleaning improvement when crystal collimators are used and can be divided into two main categories [70]: (i) *Operational settings*: These settings, schematically represented on the left side of Fig. 8, maintain the standard collimation system settings as used in normal operation, with the addition of crystal collimators set at a slightly tighter opening than the standard primary collimators. In this way, crystal collimators intercept all betatron losses and drive the cleaning performance, while the rest of the system provides the required passive protection for the machine. These settings act as a starting point for the definition of the configuration to be used in operation with heavy-ion beams. (ii) *MD settings*: In this configuration, represented on the right side of Fig. 8, the primary collimators upstream of the crystals, along with any secondary collimator located between each crystal and its corresponding absorber, are completely retracted. The crystals are placed at the same opening as the primary collimators during normal operation. These settings are explored in MD tests to assess the cleaning performance of a "pure" crystal system by removing all upstream obstacles but require additional validation before being used with high-intensity beams.

In both cases, different arrangements of the downstream TCSGs and TCLAs were tested in order to assess their effects on the global cleaning in the IR7-DS and on specific clusters of losses, following the same procedure used for previous tests with Xe ion beams [34]. The results reported in this paper focus on a single configuration for each category, with the settings (along with those for the standard system) listed in Table IV. In particular, the operational configuration is the one currently considered for the 2023 heavy-ion run.

The halo cleaning performance of the LHC collimation system is assessed by using the ADT to intentionally excite the circulating beam with white noise to generate controlled losses on the primary stage of the collimation system, be it a standard collimator or a crystal. The resulting beam losses around the ring are detected by BLMs and the loss pattern is displayed in what is commonly referred to as a *loss map*. The *cleaning inefficiency* of the system, i.e., the fraction of particles entering the collimation system that are lost at particularly sensitive locations is then used to compare the performance of the standard and crystal collimation systems. While, with standard collimation, the cleaning inefficiency is measured by normalizing all BLM signals to the highest signal recorded among the BLMs close to the primary collimators (as this is proportional to the total number of intercepted particles), this cannot be applied to crystal collimation due to the very different dynamics. Instead, the chosen normalization factor to compare the two systems is the rate of lost particles, calculated from the decrease in intensity over time observed during the beam excitation [34]. If the highest losses during a loss map are recorded at the instant t_0, the normalized signal of a specific BLM is calculated as

TABLE IV. Collimator settings (expressed in terms of beam rms σ) during cleaning measurements. For Beam 1, the asymmetric settings of the TCP left (L) and right (R) jaws (as used in normal 2018 operation with Pb ion beams) are given. The crystal collimation configuration is the same for both beams.

	Collimator settings [σ]			
Configuration	Standard Beam 1	Standard Beam 2	Crystal operational	Crystal MD
TCPs	5.5(L)–5.0(R)	5.0	5.0	Open
Upstream TCSGs	6.5	6.5	6.5	Open
Crystal	Out	Out	4.75	5.0
Downstream TCSGs	6.5	6.5	6.5	6.5
TCLAs	10.0	10.0	10.0	8.0

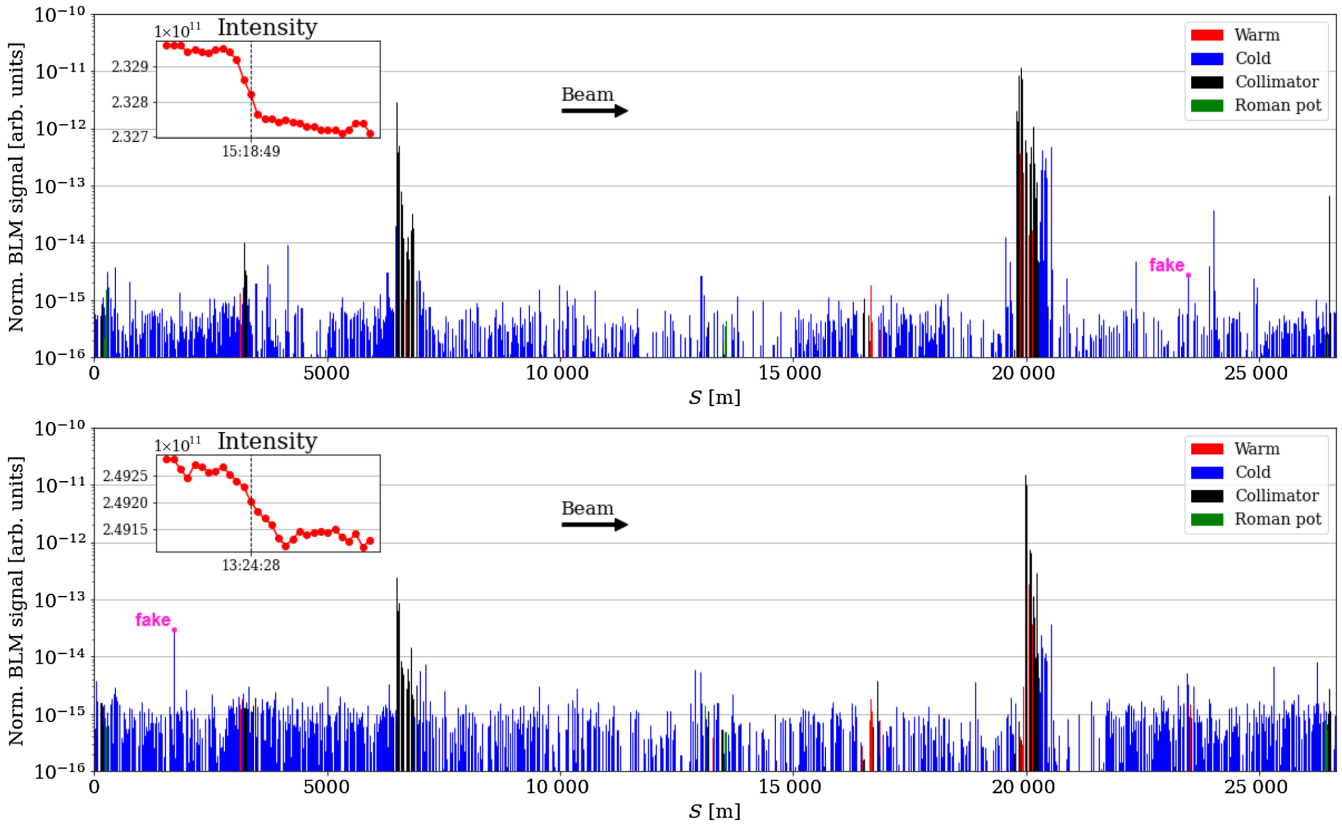

FIG. 9. Loss pattern in the whole LHC ring (normalized to the rate of lost particles) measured during a loss map for the horizontal plane of Beam 1 with 20 bunches of 6.37 Z TeV Pb ions, using standard collimation (top) and crystal collimation with MD settings (bottom). The beam intensity in number of charges as a function of time is shown in the boxed plots (note that apparent increases are due to fluctuations in the intensity reading).

$$\mathrm{BLM}_i^{\mathrm{norm}}(t_0) = \frac{\mathrm{BLM}_i(t_0) - \mathrm{BKG}_i}{|\frac{dI}{dt}(t_0)|}, \tag{3}$$

where i indicates the specific BLM considered, BKG_i is the corresponding background signal recorded before the start of the excitation, and $\frac{dI}{dt}$ is the measured intensity variation over time (the absolute value is taken to obtain a positive result since the intensity decreases during a loss map) recorded with the fast beam current transformers [71]. An example of the loss pattern observed in IR7 for the two collimation schemes (using standard and crystal MD settings, as reported in Table IV) is shown in Fig. 9. Transient signal spikes significantly above noise that do not correspond to real losses (i.e., *fake spikes*) are labeled by pink dots. These can be identified in the postprocessing as they appear and disappear typically in the span of 1 s, while real losses are proportional to the intensity loss and are consistently observed for the whole excitation. Figure 10 shows a zoom of the collimation insertion. A qualitatively cleaner pattern can be observed when crystal collimation is used. The comparison focuses on the cold IR7-DS region, which is divided into four sections identified for simplicity by the quadrupole magnets that they enclose (Q7, Q8–9, Q10–11 and Q12–13), and delimited by green dashed lines in the plots. The cleaning inefficiency η_c in each of the above regions is evaluated as the highest normalized BLM signal in the respective longitudinal range. In order to compare the performance of the crystal-based system to that of the standard system, a *local leakage ratio* (LLR_i) is defined for each region:

$$\mathrm{LLR}_i = \frac{\eta_c^{\mathrm{STD}}(i)}{\eta_c^{\mathrm{CRY}}(i)}, \tag{4}$$

where i indicates the specific IR7-DS region considered, while STD and CRY stand for standard and crystal system, respectively. With this definition, if $\mathrm{LLR}_i > 1$ for a certain region i, then the cleaning inefficiency is reduced in that region when crystals are deployed, leading to a performance improvement with respect to standard collimation. This metric is particularly useful to understand how different settings of the collimation system affect the loss pattern. However, for the purpose of evaluating the performance of the system in view of its use in operation, a more interesting aspect is the global cleaning improvement achieved across the whole IR7-DS. A *global leakage ratio* (GLR) can be defined:

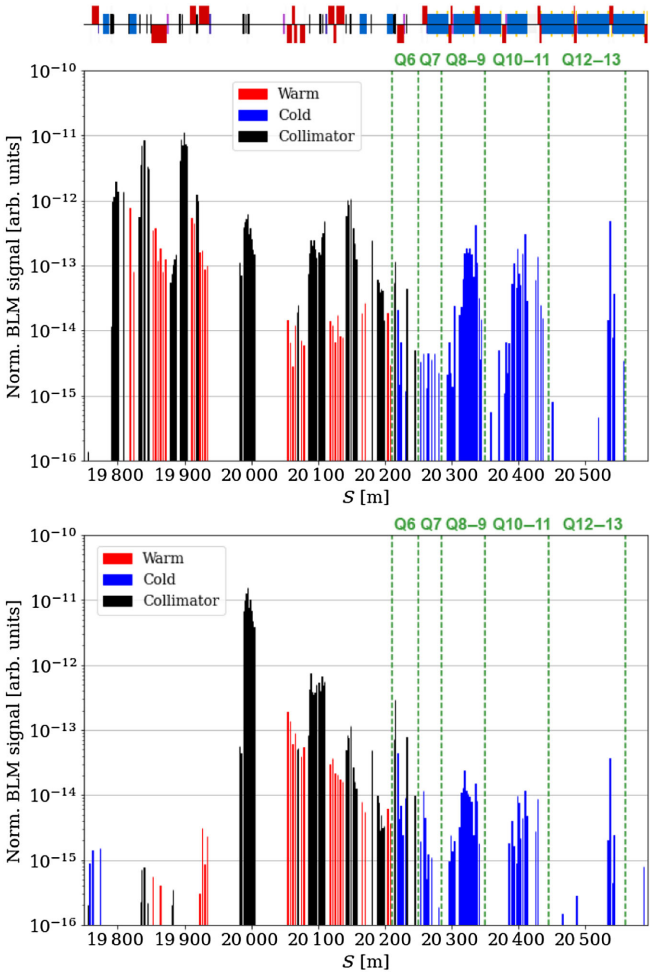

FIG. 10. Loss pattern in IR7 (normalized to the rate of lost particles) measured during a loss map for the horizontal plane of Beam 1 with 20 bunches of 6.37 Z TeV Pb ion beams using standard collimation (top) and crystal collimation with MD settings (bottom). The layout of machine elements is schematically depicted in the box plot at the top (collimators in black, dipoles in blue, and quadrupoles in red).

$$\mathrm{GLR} = \frac{\max[\eta_c^{\mathrm{STD}}]}{\max[\eta_c^{\mathrm{CRY}}]}, \tag{5}$$

which is the ratio between the maximum cleaning inefficiency measured in the whole IR7-DS with the two schemes. This quantity gives a direct measurement of the overall improvement provided by crystal collimation with respect to standard collimation. The Q6 region (upstream of Q7) is not considered for this analysis, even if noticeable losses can be observed in this area when crystals are deployed, as shown in the bottom frame of Fig. 10. In fact, the highest loss spike in this region corresponds to a BLM located upstream of the Q6 quadrupole modules. Thus, this BLM is actually detecting showers coming from upstream collimators, rather than losses on the magnets themselves. In light of these considerations, this area is presently not considered as a potential limitation in terms of magnet quench risk and is therefore not included in the cleaning inefficiency evaluation.

The measured BLM signal for the configurations described in this paper was compared against complex simulations with the goal of identifying the main contributions to each cluster of losses. This is, however, outside of the scope of this work. More details can be found in [72].

B. Achieved cleaning performance

In this section, a selection of the most relevant results of cleaning measurements with Pb ion beams will be presented. Figure 11 shows the LLR measured in loss maps for the horizontal plane of Beam 1 and Beam 2 with crystal collimation using MD and operational settings (see Table IV). In both cases, a clear improvement of the cleaning performance with respect to standard collimation in regions corresponding to dispersive peaks can be observed. In the region between Q8 and Q13, a reduction of about a factor of 8–10 is typically observed for the horizontal plane of Beam 1, and a factor of 2–3 for the horizontal plane of Beam 2. This is a consequence of the reduction of inelastic interactions of channeled particles with the atoms of the crystal, leading to reduced off-momentum losses as described above. A very efficient reduction of losses in the Q12–13 region is observed for the horizontal plane of Beam 2 with MD settings. This is especially promising since high loss peaks were observed in this region during standard ion operation in 2018 [11], and the use of crystal collimation in this configuration moved the limiting location of the IR7-DS back to the Q8–9 region, which was the limiting location observed in previous years. The Q7 region, on the other hand, shows a worsening in all cases. Leakage in this area cannot be explained by off-momentum losses, as particles escaping from the collimation insertion have yet to cross any dipoles. The origin of these losses is being looked for with dedicated simulation studies that are outside the scope of this work. However, losses at this location are smaller in absolute value than in the downstream regions (by about a factor of 10 in the operational configuration [60]), meaning that Q7 never risks to become the limiting location of the machine in terms of cleaning. This is clearly visible in Fig. 10.

The improvement in the vertical plane of each beam is significantly smaller than in the horizontal plane of the same beam. A possible explanation of this behavior could be given by the different production technologies of the crystal devices used during Run 2. As mentioned earlier, the strip crystals, installed in the horizontal plane, and the quasimosaic crystals, installed in the vertical plane, use different crystalline planes for planar channeling, leading to a different structure of the potential wells. In particular, the potential wells of quasimosaic crystals do not all have the

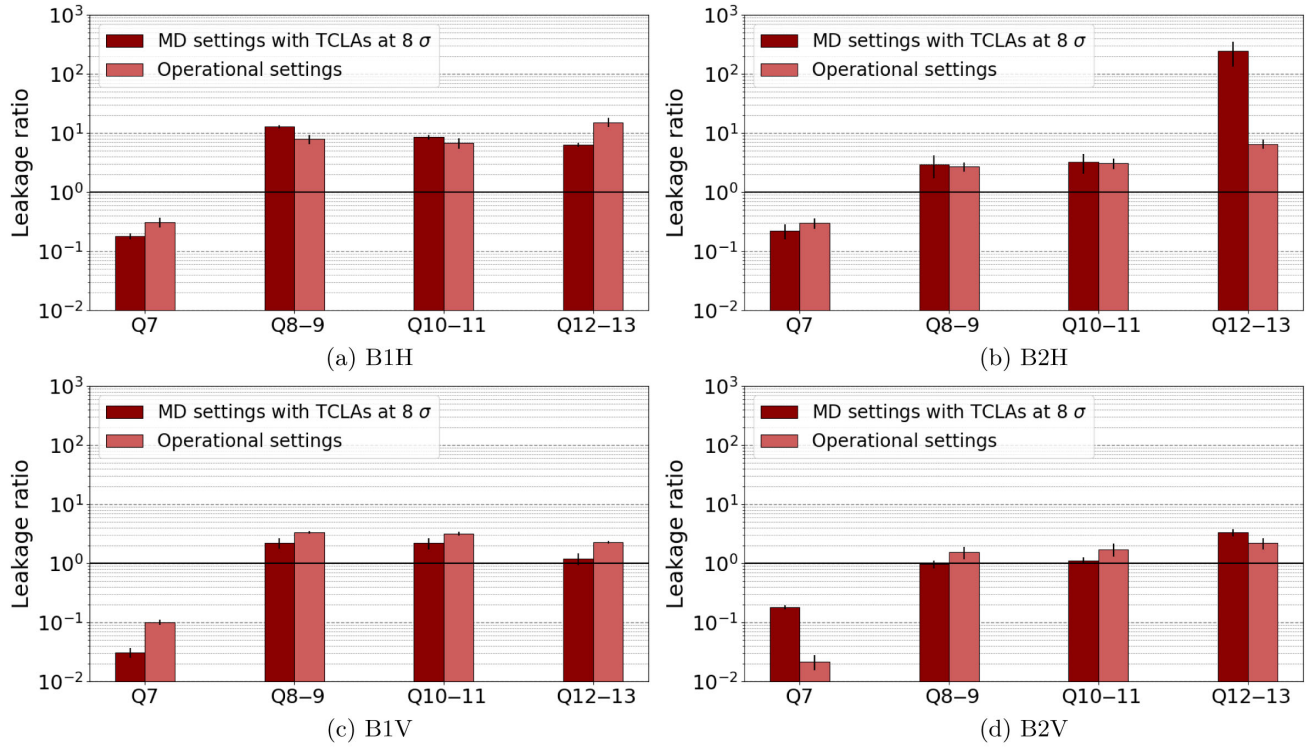

FIG. 11. Local leakage ratio between standard collimation and crystal collimation using MD and operational settings (see Table IV), measured in loss maps with 20 bunches of 6.37 Z TeV Pb ion beams using MD and operational settings. The corresponding error bars are also shown.

same width and depth. Therefore, the probability of nuclear interactions with atoms of the crystalline lattice may be higher when positively charged particles are channeled by the smallest wells, generating higher losses. This effect, already observed in measurements and simulations with proton beams [73], could be more pronounced with Pb ions due to the different interaction dynamics. Although different arrangements of downstream collimators can partially mitigate this effect, in light of these findings, it was decided to install strip crystals also in the vertical plane, taking advantage of the exchange with an updated goniometer design which was performed during the 2021–2022 Year-End Technical Stop (YETS).

During tests with operational settings, losses at the tertiary collimators (TCTs) were also monitored. These collimators protect the superconducting quadrupoles upstream of each experimental collision point of the LHC and are made of a tungsten alloy to maximize absorption at the expense of durability. For this reason, lower losses are allowed on these collimators compared to other areas of the machine [6,74]. Throughout Run 2, a number of accidental beam dumps were triggered by TCTs. Figure 12 reports, as an example, the normalized signal recorded at the TCTs during loss maps for the horizontal plane of Beam 1, showing a clear reduction when crystal collimation is used. It is worth noting that the signal recorded with crystal collimation at the TCTs in IR5 and IR8 is close to the background noise, hence the large error bars. As a result, the risk of triggering a beam dump is limited and the background leaking from these collimators and observed by the experiments is reduced. The benefit of each experiment can be quantitatively assessed only in real operation. However, a linear reduction in background levels with the reduction of TCT losses is expected [8,75].

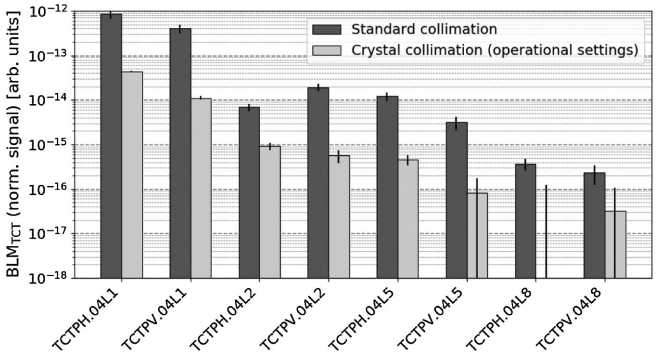

FIG. 12. Normalized BLM signal recorded at TCTs with standard and crystal collimation (operational settings) during loss maps for the horizontal plane of Beam 1 with 20 bunches of 6.37 Z TeV Pb ion beams. Note that the signal recorded for TCTPH.04L8 could not be reliably separated from the background, thus only the corresponding error bar is shown.

TABLE V. Global leakage ratio between standard collimation and crystal collimation using MD and operational settings (see Table IV), measured in tests with 6.37 Z TeV Pb ion beams.

Cleaning plane	GLR (MD settings)	GLR (operational settings)
B1H	6.4 ± 0.6	8.0 ± 1.4
B1V	1.2 ± 0.3	3.1 ± 0.1
B2H	3.8 ± 1.7	3.5 ± 0.6
B2V	1.0 ± 0.1	1.5 ± 0.4

Table V reports the GLR measured in all four planes for MD and operational settings, using the arrangement of downstream collimators that yielded the best overall results (listed in Table IV). Looking at the operational settings in particular, it is possible to see that the insertion of crystal collimators in the standard system is able to improve the cleaning of the machine by up to a factor of 8 when considering each individual plane. When considering the limiting locations among all beams and planes for the two systems (i.e., Beam 1 horizontal for standard collimation and Beam 2 vertical for crystal collimation), the overall improvement is of about a factor of 4 [60]. For both beams, the improvement provided by crystal collimators in the vertical plane is a factor of 2 or more lower than the crystal collimators in the horizontal plane of the same beam. The improvement is generally comparable or slightly lower with MD settings, which feature the complete retraction of the upstream standard collimators and a tighter aperture of the TCLAs. The specific MD configuration selected for this comparison was chosen as a tradeoff between the achieved improvement and the number of modifications with respect to the standard system. It was possible to achieve a larger improvement on selected cleaning planes with other configurations featuring more "aggressive" collimator settings, such as an even tighter aperture of the downstream TCSGs and TCLAs to better intercept leakage from the crystals and the channeled halo absorbers [60]. These settings, however, would require extensive validation to be put into operation.

It is important to note that recent findings highlighted the significant impact of the specific collimation configuration used for the standard system on the measured leakage ratio (both local and global). In particular, asymmetric settings for the jaws of the TCP in the horizontal plane of Beam 1 were used during operation with Pb ion beams in 2018 [11], to mitigate the high losses recorded at the TCTs at the expense of a slightly worse cleaning in the IR7-DS. This is why the horizontal crystal on Beam 1, despite being significantly out of specification in terms of bending angle, appears to provide the best improvement. While the qualitatively positive effect of crystal collimation is clear from the results shown so far, a definitive quantitative assessment of the achievable cleaning improvement in Run 3 can only be done with the final operational configuration.

V. FIRST USE OF CRYSTALS WITH HIGH-INTENSITY PB ION BEAMS

Increasing the intensity of the circulating beams poses a number of operational challenges in terms of heating, beam instabilities, and more. Since these aspects cannot be easily studied and predicted in simulations, an empirical assessment is performed instead. For this reason, LHC operation with the high-intensity beams required by the experiments is always preceded by a careful *intensity ramp-up*, during which the number of circulating bunches is increased in carefully monitored steps. Before moving to the next step, the full and proper functioning of all systems (e.g., magnet protection, radiofrequency, beam instrumentation, collimation, feedback, beam dump, injection, etc.) must be verified. At the end of each step, when all the system checks have been successfully performed, a few hours can be dedicated to specific tests before the beams are dumped and replaced with fresh ones.

These *end-of-fill* tests offered the opportunity to successfully deploy crystal collimation with up to 648 circulating bunches of Pb ions, for a maximum total intensity of 3.76×10^{12} charges [60]. The ability to verify the stability of the system in such challenging conditions was an extremely important milestone on the path toward the validation of crystal collimation for use in operation. In particular, it is important to note that the setup of the crystal collimation system for these studies was very efficient, demonstrating the high reproducibility of the devices. For each insertion of the crystals in the beam line, a quick angular scan was performed to check if the optimal channeling orientation was maintained over long time intervals, using results from the initial setup as a reference starting point. Figure 13 shows an example of the horizontal crystal on Beam 1 after

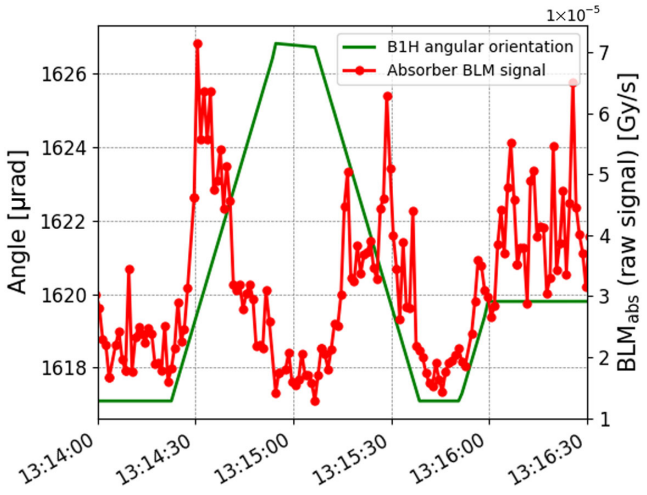

FIG. 13. Example of an angular scan around the reference optimal orientation of the crystal collimator on the horizontal plane of Beam 1 after its insertion with 648 circulating bunches of Pb ions. The reference of 1613 μrad from the previous insertion was adjusted by 7 μrad.

TABLE VI. Optimal channeling orientation for each crystal collimator in the different insertions with Pb ion beams in 2018. The date and number of circulating bunches are also reported for each test.

Date	November 4, 2018	November 7, 2018	November 9, 2018	November 19, 2018	November 27, 2018
Number of bunches	25	20	20	648	20
B1H orientation (μrad)	1605	1609	1613	1620	1620
B1V orientation (μrad)	2538	2537	2537	2528	2532
B2H orientation (μrad)	−3466	−3470	−3470	−3475	−3476
B2V orientation (μrad)	−188	−195	−195	...	310

its insertion with 648 circulating bunches. Optimal channeling conditions are clearly identified by an increase of the BLM signal at the secondary collimator that catches the deflected halo, allowing the reference orientation found in previous tests to be verified, and corrections to be applied if necessary. The whole procedure only required a couple of minutes. This strategy proved to be effective even without artificial excitation, thanks to the elevated losses generated by high-intensity beams. The optimal orientation found for each crystal in each test is reported in Table VI. Minor adjustments were needed between subsequent insertions. It is planned to deploy dedicated tools to automatically optimize the orientation of crystal collimators by performing small angular scans [76,77]. The only device requiring major adjustments was the vertical crystal of Beam 2, as the reference position of its goniometer was lost between consecutive measurement sessions and could only be reestablished during a dedicated test. This was a known limitation of the goniometer design used until 2018. All four crystal collimator assemblies have now been replaced with an updated goniometer design to address this problem and ensure more reliable and stable performance.

A stable cleaning performance was observed in loss maps performed during end-of-fill tests, and the temperature of the crystal collimator devices was continually monitored showing no evidence of dangerous heating from the high-intensity beams. Cleaning measurements were also performed with the crystals in the amorphous

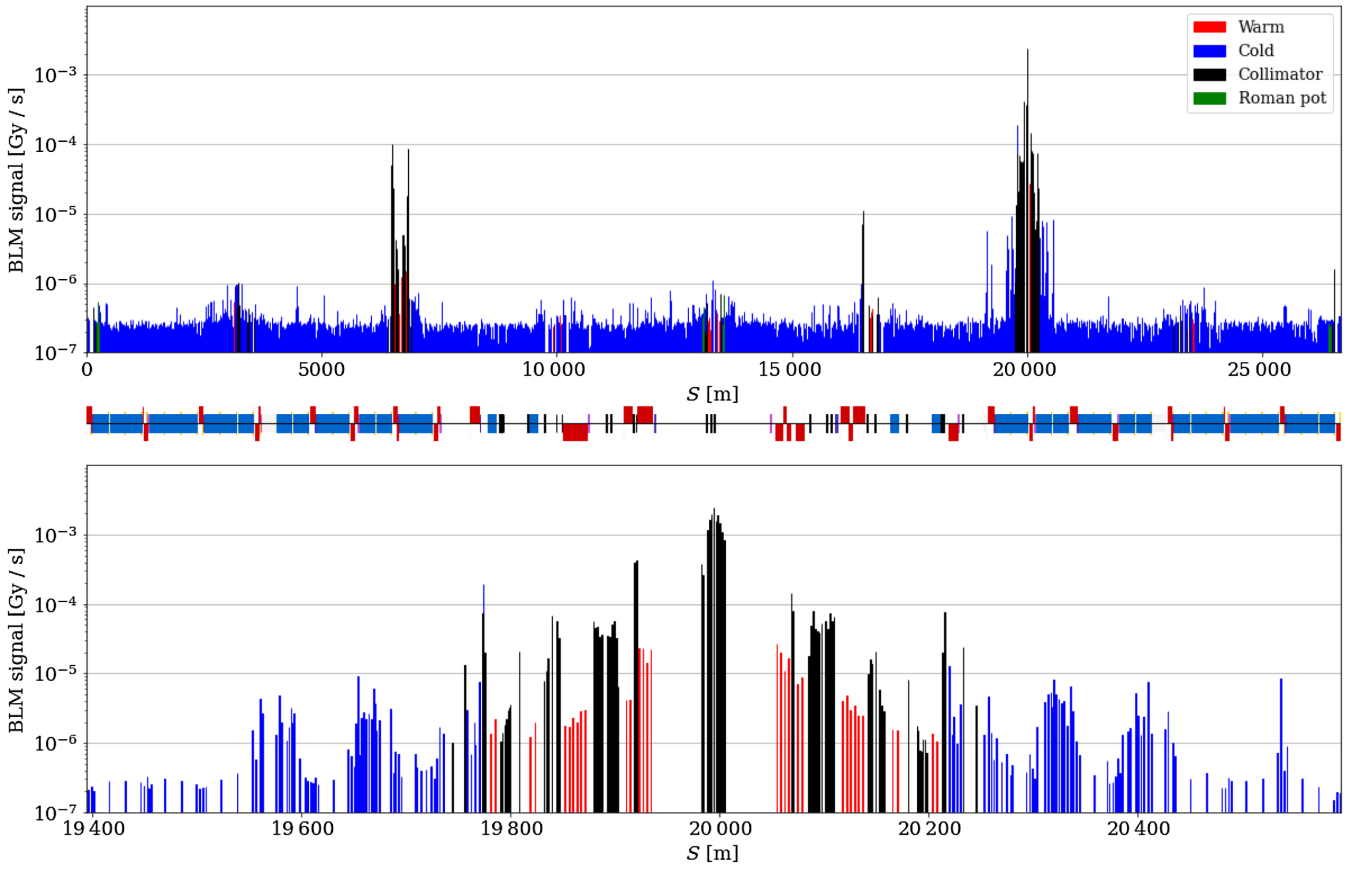

FIG. 14. Loss pattern observed while generating sustained losses on all four planes at the same time, with 20 circulating Pb ion bunches and using crystal collimation with MD settings. The full ring (top) and the IR7 region (bottom) are shown.

orientation, to assess the effect of misalignments through changes in the beam angle or other accidental scenarios. In such conditions, the cleaning performance in the DS decreases by up to a factor of 2–2.5 compared to standard collimation, with the crystal completely losing its capability of deflecting incoming halo particles, behaving just like a thin standard collimator. This stresses the importance of continuously monitoring the orientation of the crystal collimators to ensure that channeling conditions are maintained during operations. To this end, a set of dedicated tools capable of recognizing the loss of channeling conditions from changes in the loss pattern are currently being developed and tested, and will be deployed in future ion runs [76,77].

A number of additional tests aimed at ensuring that safe operation can be guaranteed during standard operation were also carried out, such as channeling while generating high losses in all planes at the same time with 20 bunches (with no abnormal peaks observed and generally a very clean loss pattern around the ring, as shown in Fig. 14), an asynchronous beam dump test and stable channeling for about 2 h with 648 bunches. It was also possible to maintain optimal channeling while orbit corrections were applied, as well as during the squeeze (i.e., when the beam size is reduced at the interaction points to prepare for collisions). The positive outcome of all these tests together with the experience gathered with crystal collimation over the entirety of Run 2 resulted in this innovative collimation scheme being included as the baseline for ion collimation in the HL-LHC era.

VI. CONCLUSIONS AND OUTLOOK

As part of the R&D effort to improve beam collimation for HL-LHC, an extensive campaign of experimental tests and operational investigations was carried out to assess the feasibility of crystal collimation of high-intensity hadron beams. The successful outcome of these tests over the entirety of Run 2, together with the results gathered in 2018 and summarized in this paper, demonstrated the capability of this innovative collimation scheme to improve the beam cleaning with 6.37 Z TeV Pb ion beams at the LHC by up to a factor of 8 when looking at single planes, and up to a factor of 4 when looking at the overall limiting plane. Crystal collimators were used for the very first time with high-intensity Pb ion beams (up to 648 bunches), showing a cleaning gain similar to low-intensity tests and no unexpected detrimental intensity-related effects such as instabilities or heating. In view of possible deployment during Run 3, a first proposal for operational settings was elaborated, inserting the crystals in the present collimation system to achieve a significant cleaning improvement in the IR7 dispersion suppressor region. A generally cleaner pattern around the full LHC ring and a reduction of losses at the tertiary collimators of up to an order of magnitude was also observed.

The similarities of the LHC ion configuration planned for operation during Run 3 (i.e., collimators at the same settings, only slightly higher energy, same optics in IR7) gave enough confidence to propose crystal collimation as part of the baseline program of the HL-LHC upgrade at the end of 2019. Other aspects crucial for operation, such as the preparation and deployment of ramp functions to maintain channeling conditions during the energy ramp, were addressed in the first tests with proton beams in Run 2 [34,60] and during the proton commissioning at the beginning of Run 3 with promising results.

A longer-term follow-up point is related to the potential limitations of the current primary crystal collimators as single-sided devices. The need to install additional crystals on the opposite side of the beam pipe for each cleaning plane will be reevaluated based on operational experience gained in future ion runs.

ACKNOWLEDGMENTS

Crystal collimation tests at the LHC are carried out with the support of the HL-LHC Project. The authors would like to thank the UA9 collaboration for their long-standing contribution to the crystal collimation concept and its validation, as well as for providing and characterizing the bent crystals prior to their installation in the LHC. The crystals were manufactured by INFN-Ferrara and PNPI. Contributions from the CERN BE-ABP, BE-CEM, BE-OP, and SY-STI groups are also kindly acknowledged.

[1] O. Brüning, P. Collier, P. Lebrun, S. Myers, R. Ostojic, J. Poole, and P. Proudlock, LHC design report Vol. 1: The LHC main ring, CERN Yellow Reports: Monographs, 2004, http://dx.doi.org/10.5170/CERN-2004-003-V-1.

[2] J. Jowett, Colliding heavy ions in the LHC, in *Proceedings of 9th International Particle Accelerator Conference, IPAC-2018, Vancouver, Canada* (JACoW, Geneva, Switzerland, 2018), http://dx.doi.org/10.18429/JACoW-IPAC2018-TUXGBD2.

[3] M. Schaumann, R. Alemany-Fernandez, P. Baudrenghien, T. Bohl, C. Bracco, R. Bruce *et al.*, First Xenon-Xenon collisions in the LHC, in *Proceedings of 9th International Particle Accelerator Conference, IPAC-2018, Vancouver, Canada* (JACoW, Geneva, Switzerland, 2018), http://dx.doi.org/10.18429/JACoW-IPAC2018-MOPMF039.

[4] R.W. Assmann, O. Aberle, G. Bellodi, A. Bertarelli, C. Bracco, H. Braun *et al.*, The final collimation system for the LHC, in *Proceedings of the 10th European Particle Accelerator Conference, Edinburgh, Scotland, 2006* (2006), p. 986, Report No. CERN-LHC-PROJECT-REPORT-919.

[5] R. Bruce, R. W. Assmann, V. Boccone, C. Bracco, M. Brugger, M. Cauchi *et al.*, Simulations and measurements of beam loss patterns at the CERN Large Hadron Collider, Phys. Rev. ST Accel. Beams **17**, 081004 (2014).

[6] R. Bruce, C. Bracco, R. De Maria, M. Giovannozzi, A. Mereghetti, D. Mirarchi, S. Redaelli, E. Quaranta, and B. Salvachua, Reaching record-low β^* at the CERN Large Hadron Collider using a novel scheme of collimator settings and optics, Nucl. Instrum. Methods Phys. Res., Sect. A **848**, 19 (2017).

[7] G. Valentino, G. Baud, R. Bruce, M. Gasior, A. Mereghetti, D. Mirarchi *et al.*, Final implementation, commissioning, and performance of embedded collimator beam position monitors in the Large Hadron Collider, Phys. Rev. Accel. Beams **20**, 081002 (2017).

[8] R. Bruce, M. Huhtinen, A. Manousos, F. Cerutti, L. Esposito, R. Kwee-Hinzmann *et al.*, Collimation-induced experimental background studies at the CERN Large Hadron Collider, Phys. Rev. Accel. Beams **22**, 021004 (2019).

[9] G. Azzopardi, B. Salvachua Ferrando, G. Valentino, S. Redaelli, and A. Muscat, Operational results on the fully-automatic LHC collimator alignment, Phys. Rev. Accel. Beams **22**, 093001 (2019).

[10] A. Gorzawski, A. Abramov, R. Bruce, N. Fuster Martinez, M. Krasny, J. Molson, S. Redaelli, and M. Schaumann, Collimation of partially stripped ions in the CERN Large Hadron Collider, Phys. Rev. Accel. Beams **23**, 101002 (2020).

[11] N. Fuster, R. Bruce, F. Cerutti, R. De Maria, P. D. Hermes, A. Lechner *et al.*, Simulations of heavy-ion halo collimation at the CERN Large Hadron Collider: Benchmark with measurements and cleaning performance evaluation, Phys. Rev. Accel. Beams **23**, 111002 (2020).

[12] N. Fuster Martinez, R. W. Assmann, R. Bruce, M. Giovannozzi, P. D. Hermes, A. Mereghetti, D. Mirarchi, S. Redaelli, and J. Wenninger, Beam-based aperture measurements with movable collimator jaws as performance booster of the CERN Large Hadron Collider, Eur. Phys. J. Plus **137**, 305 (2022).

[13] S. Redaelli, Beam cleaning and collimation systems, in *CERN Yellow Reports* (2016), Vol. 2, http://dx.doi.org/10.5170/CERN-2016-002.403.

[14] S. Redaelli, R. Bruce, A. Lechner, and A. Mereghetti, Chapter 5: Collimation system, in CERN Yellow Reports Monographs (2020), Vol. **10**, pp. 87–114, Report No. CERN-2020-010, http://dx.doi.org/10.23731/CYRM-2020-0010.

[15] O. Brüning and L. Rossi, The High Luminosity Large Hadron Collider, in *Advanced Series on Directions in High Energy Physics* (2015), http://dx.doi.org/10.1142/9581.

[16] I. Béjar Alonso, O. Brüning, P. Fessia, L. Rossi, L. Tavian, and M. Zerlauth, High-Luminosity Large Hadron Collider (HL-LHC): Technical design report, in CERN Yellow Reports: Monographs (2020), Report No. CERN-2020-010, http://dx.doi.org/10.23731/CYRM-2020-0010.

[17] R. Bruce, M. Jebramcik, J. Jowett, T. Mertens, and M. Schaumann, Performance and luminosity models for heavy-ion operation at the CERN Large Hadron Collider, Eur. Phys. J. Plus **136**, 745 (2021).

[18] The ALICE Collaboration, The ALICE experiment at the CERN LHC, J. Instrum. **3**, S08002 (2008).

[19] P. D. Hermes, R. Bruce, J. Jowett, S. Redaelli, B. Salvachua Ferrando, G. Valentino, and D. Wollman, Measured and simulated heavy-ion beam loss patterns at the CERN Large Hadron Collider, Nucl. Instrum. Methods Phys. Res., Sect. A **819**, 73 (2016).

[20] H. H. Braun, R. W. Assmann, A. Ferrari, J. B. Jeanneret, J. M. Jowett, and I. A. Pshenichnov, Collimation of heavy ion beams in LHC, in *Proceedings of the 9th European Particle Accelerator Conference, Lucerne, 2004* (EPS-AG, Lucerne, 2004), p. 551.

[21] H. H. Braun, A. Fassò, A. Ferrari, J. M. Jowett, P. R. Sala, and G. I. Smirnov, Hadronic and electromagnetic fragmentation of ultrarelativistic heavy ions at LHC, Phys. Rev. ST Accel. Beams **17**, 021006 (2014).

[22] W. Fisher, E. Aschenauer, E. Beebe, M. Blaskiewicz, K. Brown *et al.*, eRHIC in electron-ion operation, in *Proceedings of IPAC'19, Melbourne, VIC, Australia* (2019), http://dx.doi.org/10.18429/JACoW-IPAC2019-MOPRB072.

[23] J. Stadlmann, H. Kollmus, E. Mustafin, I. Petzenhauser, P. Spiller *et al.*, Collimation and material science studies COLMAT at GSI, in *Proceedings of the International Particle Accelerator Conference, Kyoto, Japan, 2010* (ICR, Kyoto, 2010).

[24] N. Fuster Martinez, A. Abramov, G. Azzopardi, A. Gorzawski, E. Belli, C. Boscolo-Meneguolo *et al.*, Run 2 collimation overview, in *Proceedings of 9th LHC Operations Evian Workshop, Evian-les-Bains, France* (2019), pp. 149–164, Report No. CERN-ACC-2019-059.

[25] E. Skordis, Radiation impact of collimation beam losses in the LHC and HL-LHC, Ph.D. thesis, University of Liverpool, UK, 2019.

[26] C. Bahamonde *et al.*, Energy deposition from collimation losses in the DS region at P7, in *8th HL-LHC Collaboration Meeting* (CERN, Geneva, Switzerland, 2018), https://indico.cern.ch/event/742082/contributions/3085132/.

[27] R. Bruce, T. Argyropoulos, H. Bartosik, R. De Maria, N. Fuster-Martinez, M. A. Jebramik *et al.*, *HL-LHC operational scenario for Pb-Pb and p-Pb operation* (CERN, Geneva, Switzerland, 2020), Report No. CERN-ACC-2020-0011.

[28] R. Bruce, 2023 Pb-Pb run: Plans, status and preparations, in *2023 LHC heavy-ion preparation meeting* (CERN, Geneva, Switzerland, 2023), https://indico.cern.ch/event/1285380/.

[29] R. Bruce, A. Marsili, and S. Redaelli, Cleaning performance with 11T dipoles and local dispersion suppressor collimation at the LHC, in *Proceedings of 5th International Particle Accelerator Conference, IPAC-2014, Dresden, Germany* (JACoW, Geneva, Switzerland, 2014).

[30] A. Lechner, B. Auchmann, R. Bruce, F. Cerutti, P. P. Granieri, A. Marsili, S. Redaelli *et al.*, Power deposition in LHC magnets with and without dispersion suppressor collimators downstream of the betatron cleaning insertion, in *Proceedings of 5th International Particle Accelerator Conference, IPAC-2014, Dresden, Germany* (JACoW, Geneva, Switzerland, 2014), https://doi.org/10.18429/JACoW-IPAC2014-MOPRO021.

[31] C. Bahamonde, A. Lechner, and R. Rossi, Crystal channeling of ions on different TCSG materials, in *LHC Collimation Upgrade Specification Meeting* (CERN,

Geneva, Switzerland, 2018), https://indico.cern.ch/event/740297/.

[32] D. Mirarchi, S. Redaelli, R. Rossi, and W. Scandale, Crystal collimation system: Concept and layouts, in *HL-LHC Crystal Collimation Day* (CERN, Geneva, Switzerland, 2018), https://indico.cern.ch/event/752062/contributions/3114826/.

[33] S. Redaelli, M. Butcher, C. Barreto, R. Losito *et al.*, First observation of ion beam channeling in bent crystals at multi-TeV energies, Eur. Phys. J. C **81**, 142 (2021).

[34] R. Rossi, Experimental assessment of crystal collimation at the Large Hadron Collider, Ph.D. thesis, Università La Sapienza di Roma, Italy, Report No. CERN-THESIS-2017-424, 2017.

[35] HL-LHC Crystal Collimation Day meeting, CERN, Geneva, Switzerland (2018), https://indico.cern.ch/event/752062/.

[36] S. Redaelli, Status of HL-LHC collimation upgrade in LS2 and future plans, in *10th HL-LHC Collaboration Meeting, Uppsala, Sweden* (2020), https://indico.cern.ch/event/937797/contributions/3951885/.

[37] V. M. Biryukov, Computer simulation of dislocation dechanneling in bent crystals at tera-electron-volt energies, Phys. Rev. E **52**, 2045 (1995).

[38] J. Lindhard, Influence of crystal lattice on motion of energetic charged particles, Mat. Fys. Medd. K. Dan. Vidensk. Selsk **34**, 14 (1965), https://gymarkiv.sdu.dk/MFM/kdvs/mfm%2030-39/mfm-34-14.pdf.

[39] E. N. Tsyganov, Some aspects of the mechanism of a charge particle penetration through a monocrystal, Fermilab, Batavia, IL, Report No. FERMILAB-TM-0682, 1976.

[40] V. M. Biryukov, Y. A. Chesnokov, and V. I. Kotov, *Crystal Channeling and Its Application at High-Energy Accelerators* (Springer Science & Business Media, 2013).

[41] K. Elsener, G. Fidecaro, M. Gyr, W. Herr, J. Klem, U. Mikkelsen, S.P. Møller, E. Uggerhøj, G. Vuagnin, and E. Weisse, Proton extraction from the CERN SPS using bent silicon crystals, Nucl. Instrum. Methods Phys. Res., Sect. B **119**, 215 (1996).

[42] A. G. Afonin, V. T. Baranov, V. M. Biryukov, M. B. H. Breese, V. N. Chepegin *et al.*, High-efficiency beam extraction and collimation using channeling in very short bent crystals, Phys. Rev. Lett. **87**, 094802 (2001).

[43] F. M. Velotti, M. Di Castro, L. S. Esposito, M. Fraser, S. Gilardoni *et al.*, Exploitation of crystal shadowing via multi-crystal array, optimizers and reinforcement learning, in *Proceedings of 13th International Particle Accelerator Conference, IPAC-2022, Bangkok, Thailand* (JACoW, Geneva, Switzerland, 2022), pp. 1707–1710. http://dx.doi.org/10.18429/JACoW-IPAC2022-WEPOST013.

[44] F. M. Velotti, M. Fraser, P. A. Arrutia Sota, M. Calviani, M. Di Castro *et al.*, Demonstration of nonlocal crystal shadowing at the CERN SPS, in *Proceedings of 14th International Particle Accelerator Conference, IPAC-2023, Venice, Italy* (JACoW, Geneva, Switzerland, 2023), https://doi.org/10.18429/JACoW-IPAC2023-MOPA098.

[45] R. A. Carrigan, Jr., T. E. Toohig, and E. N. Tsyganov, Beam extraction from TeV accelerators using channeling in bent crystals, Nucl. Instrum. Methods Phys. Res., Sect. B **48**, 167 (1990).

[46] C. Hadjidakis, D. Kikola, J. P. Lansberg, L. Massacrier, M. G. Echevarria *et al.*, A fixed-target programme at the LHC: Physics case and projected performances for heavy-ion, hadron, spin and astroparticle studies, Phys. Rep. **911**, 1 (2021).

[47] R. P. Fliller, A. Drees, D. Gassner, L. Hammons, G. McIntyre, S. Peggs, D. Trbojevic, V. Biryukov, Y. Chesnokov, and V. Terekhov, RHIC crystal collimation, Nucl. Instrum. Methods Phys. Res., Sect. B **234**, 47 (2005).

[48] R. P. Fliller, A. Drees, D. Gassner, L. Hammons, G. McIntyre *et al.*, Results of bent crystal channeling and collimation at the Relativistic Heavy Ion Collider, Phys. Rev. ST Accel. Beams **9**, 013501 (2006).

[49] V. D. Shiltsev, Experience with crystals at Fermilab accelerators, Int. J. Mod. Phys. A **34**, 1943007 (2019).

[50] R. Assmann, S. Redaelli, W. Scandale *et al.*, Optics study for a possible crystal-based collimation system for the LHC, in *Proceedings of the 10th European Particle Accelerator Conference, Edinburgh, Scotland, 2006* (EPS-AG, Edinburgh, Scotland, 2006), Report No. CERN-LHC-PROJECT-REPORT-918.

[51] W. Scandale, G. Arduini, R. W. Assmann, C. Bracco, M. Butcher, F. Cerutti *et al.*, Feasibility of crystal-assisted collimation in the CERN accelerator complex, Int. J. Mod. Phys. A **37**, 2230004 (2022).

[52] W. Scandale, G. Arduini, M. Butcher, F. Cerutti, M. Garattini, S. Gilardoni *et al.*, Observation of channeling for 6500 GeV/c protons in the crystal assisted collimation setup for LHC, Phys. Lett. B **758**, 129 (2016).

[53] D. Mirarchi, V. Avati, R. Bruce, M. Butcher, M. D'Andrea, M. Di Castro *et al.*, Reducing beam-related background on forward physics detectors using crystal collimation at the Large Hadron Collider, Phys. Rev. Appl. **14**, 064066 (2020).

[54] W. Scandale, Crystal-based collimation in modern hadron colliders, Int. J. Mod. Phys. A **25**, 70 (2010).

[55] W. Scandale, G. Arduini, M. Butcher, F. Cerutti, S. Gilardoni *et al.*, Optimization of the crystal assisted collimation of the SPS beam, Phys. Lett. B **726**, 182 (2013).

[56] D. Mirarchi, Crystal collimation for LHC, Ph.D. thesis, Imperial College London, UK, Report No. CERN-THESIS-2015-099, 2015.

[57] V. Previtali, Performance evaluation of a crystal-enhanced collimation system for the LHC, Ph.D. thesis, École polytechnique fédérale de Lausanne, Switzerland, Report No. CERN-THESIS-2010-133, 2010.

[58] S. Montesano, F. Galluccio, J. Lendaro, F. Loprete, R. Losito, A. Masi *et al.*, Installation of the LUA9 equipment in IR7 of the LHC, CERN, Geneva, Switzerland, Report No. LHC-TEC-EC-0001, 2014.

[59] S. Redaelli, A. Masi, D. Mirarchi, S. Montesano, and R. Rossi, Installation in IR7 of primary crystal collimators (TCPC) on Beam 2, CERN, Geneva, Switzerland, Report No. LHC-TC-EC-0008, 2016.

[60] M. D'Andrea, Applications of crystal collimation to the CERN Large Hadron Collider (LHC) and its High-Luminosity upgrade project (HL-LHC), Ph.D. thesis, Università degli Studi di Padova, Italy, Report No. CERN-THESIS-2021-022, 2021.

[61] B. Dehning, E. Effinger, J. Emery, G. Ferioli, G. Guaglio, E. B. Holzer *et al.*, The LHC beam loss measurement system, in *Proceedings of the 22nd Particle Accelerator Conference, PAC-2007, Albuquerque, NM* (2021), p. 4192, http://dx.doi.org/10.1109/PAC.2007.4439980.

[62] G. Valentino, A. A. Nosych, R. Bruce, M. Gasior, D. Mirarchi, S. Redaelli, B. Salvachua Ferrando, and D. Wollmann, Successive approximation algorithm for beam-position-monitor-based LHC collimator alignment, Phys. Rev. ST Accel. Beams **17**, 021005 (2014).

[63] M. Soderen, J. Komppula, G. Kotzian, S. Rains, and D. Valuch, ADT and Obsbox in LHC Run 2, plans for LS2, in *Proceedings of 9th LHC Operations Evian Workshop, Evian-les-Bains, France* (2019), pp. 165–171.

[64] SixTrack website, http://sixtrack.web.cern.ch/

[65] F. Schmidt *et al.*, *SixTrack User's Reference Manual Version 5.4.3* (CERN, Geneva, Switzerland, 2019).

[66] R. De Maria *et al.*, SixTrack Version 5: Status and new developments, J. Phys. Conf. Ser. **1350**, 012129 (2019).

[67] D. Mirarchi, S. Redaelli, and W. Scandale, Crystal implementation in SixTrack for proton beams, in *CERN Yellow Reports Conference Proceedings* (2018), Vol. 2, pp. 91–108, https://doi.org/10.23732/CYRCP-2018-002.91.

[68] Y. M. Ivanov, A. A. Petrunin, V. V. Skorobogatov, Y. A. Gavrikov, A. V. Gelamkov *et al.*, Volume reflection of a proton beam in a bent crystal, Phys. Rev. Lett. **97**, 144801 (2006).

[69] A. Wegscheider, A. Langner, R. Tomas, and A. Franchi, Analytical *N* beam position monitor method, Phys. Rev. Accel. Beams **20**, 111002 (2017).

[70] M. D'Andrea, R. Bruce, M. Di Castro, F. Galluccio, I. Lamas Garcia, A. Masi *et al.*, Crystal collimation of 20 MJ heavy-ion beams at the HL-LHC, in *Proceedings of 12th International Particle Accelerator Conference, Campinas, SP, Brazil* (JACoW, Geneva, Switzerland, 2021), pp. 2644–2647, http://dx.doi.org/10.18429/JACoW-IPAC2021-WEPAB023.

[71] D. Belohrad, L. K. Jensen, O. R. Jones, M. Ludwig, and J. J. Savioz, The LHC fast BCT system: A comparison of design parameters with initial performance, CERN, Geneva, Switzerland, Report No. CERN-BE-2010-010, 2010.

[72] J. B. Potoine, R. Bruce, R. Cai, F. Cerutti, M. D'Andrea, L. Esposito *et al.*, Power deposition studies for standard and crystal-assisted heavy ion collimation in the CERN Large Hadron Collider, Phys. Rev. Accel. Beams **26**, 093001 (2023).

[73] W. Scandale, G. Arduini, M. Butcher, F. Cerutti, M. Garattini *et al.*, High-efficiency deflection of high energy protons due to channeling along the (110) axis of a bent silicon crystal, Phys. Lett. B **760**, 826 (2016).

[74] R. Bruce, R. W. Assmann, and S. Redaelli, Calculations of safe collimator settings and β^* at the CERN Large Hadron Collider, Phys. Rev. ST Accel. Beams **18**, 061001 (2015).

[75] R. Bruce, R. W. Assmann, V. Boccone, G. Bregliozzi, H. Burkhardt, F. Cerutti *et al.*, Sources of machine-induced background in the ATLAS and CMS detectors at the CERN Large Hadron Collider, Nucl. Instrum. Methods Phys. Res., Sect. A **729**, 825 (2013).

[76] M. D'Andrea, G. Ricci *et al.*, Prospects to apply machine learning to optimize the operation of the crystal collimation system at the LHC, in *Proceedings of the 13th International Particle Accelerator Conference, IPAC-2022, Bangkok, Thailand* (JACoW, Geneva, Switzerland, 2022), pp. 1362–1365, http://dx.doi.org/10.18429/JACoW-IPAC2022-TUPOTK061.

[77] D. Mirarchi, O. Andreassen, R. Bruce, R. Cai, M. Di Castro *et al.*, Operational handling of crystal collimation at the LHC, in *Proceedings of the 14th International Particle Accelerator Conference, IPAC-2023, Venice, Italy* (JACoW, Geneva, Switzerland, 2023), https://doi.org/10.18429/JACoW-IPAC2023-MOPL022.